Effect of TiO_2 Addition in Ladle Slag on Evolution of Nonmetallic Inclusions in Ti-Bearing Al-Killed Steel

GUANGYU HAO, ZHIYIN DENG, XIAOFENG LIU, and MIAOYONG ZHU

To investigate the effect of TiO_2 in refining slag on the nonmetallic inclusions in Ti-bearing Al-killed steel, industrial studies are conducted with and without TiO_2 addition in refining slags. It is found that a suitable addition of TiO_2 (around 5 pct) can improve the fluidity of the slag. When using TiO_2-containing slag, the Ti content in steel increases to 72 ppm after LF refining due to [Ti]-[O] equilibrium, and the yield of Ti-Fe alloy also climbs from 86.5 to 96.3 pct in RH refining even with a lower addition amount. The inclusions generally transform from Al_2O_3 into solid $MgO\text{-}Al_2O_3$ and even liquid $CaO\text{-}Al_2O_3$ inclusions. Although a small amount of TiO_x is generated in inclusions at the middle stage of LF refining due to the effect of TiO_2-containing slag, solid $MgO\text{-}Al_2O_3$ inclusions are still the dominant inclusions in steel after RH refining. Therefore, the suitable addition of TiO_2 does not evidently influence the evolution of inclusions. As a result, it can hardly weaken the removal efficiency of inclusions, while the cleanliness of steel is in fact improved. Lower total oxygen and nitrogen contents are obtained, and the number density of inclusions decreases from 31.7 mm^{-2} to 25.0 mm^{-2}.

https://doi.org/10.1007/s11663-024-03181-4
© The Minerals, Metals & Materials Society and ASM International 2024

I. INTRODUCTION

TITANIUM (Ti) is widely used to improve steel properties, such as strength, ductility, formability and weldability.[1–3] On the other hand, due to its high affinity to oxygen, the addition of Ti to liquid steel can affect the compositions of the inclusions in steel,[4–6] even leading to some production problems, such as clogging of submerged entry nozzles (SEN).[7–9]

A large number of studies were conducted to investigate the effect of Ti on the formation and evolution of inclusions in Ti-bearing steel grades, *e.g.*, gear steel,[5,10] IF steel[7,11,12] and stainless steel.[13,14] In the case of Ti-bearing gear steel, the authors[5] found that before the addition of Ti, the inclusions transformed along the route of "$Al_2O_3 \rightarrow MgO\text{-}Al_2O_3 \rightarrow CaO\text{-}Al_2O_3$", whereas the inclusions changed into $MgO\text{-}Al_2O_3\text{-}TiO_x$ or $CaO\text{-}Al_2O_3\text{-}TiO_x$ after Ti addition. For low carbon and ultra-low carbon steels (IF steel), due to the high FeO content, the effect of the slag on the evolution of the inclusions is relatively weak. As a result, the inclusions are dominated by Al_2O_3 and $Al_2O_3\text{-}TiO_x$.[7] In terms of stainless steel, the evolution of inclusions was generally different from that of conventional steel grades, because argon oxygen decarburization furnaces (AOD) are often used in the production process. Chen *et al.*[13] reported that $CaO\text{-}Al_2O_3\text{-}MgO\text{-}TiO_x$ inclusions were observed after the addition of Ti in stainless steel grade 321. In the laboratory study of Li *et al.*[14] when 0.02 pct Ti was added in the steel, Al_2O_3-TiN inclusions were detected. If the Ti content in the steel further climbed to 0.05 pct or 0.12 pct, TiN and Al_2O_3-TiN were the dominant inclusions. According to these studies, it can be concluded that the types of inclusions in Ti-bearing steel grades are strongly influenced by Ti content, and a higher Ti content may result in a higher TiO_x content in the inclusions.

During the secondary refining process, due to thermodynamic equilibrium, the dissolved Ti in steel should transfer to the slag, increasing the content of TiO_x in the slag. This has been proved by industrial practice.[13,15] Therefore, TiO_x-containing slags may be directly considered for the refining of Ti-bearing steel grades to increase the yield of Ti alloys. Previous studies of the authors[16,17] investigated the properties of TiO_2-containing refining slags, and they found that suitable addition of TiO_2 to refining slags could lower the melting point and the viscosity of the slags, thus improving the fluidity of the slags. In addition, the degradation behaviors of MgO refractory by TiO_2-containing slag

GUANGYU HAO, ZHIYIN DENG, and MIAOYONG ZHU are with the Key Laboratory for Ecological Metallurgy of Multimetallic Mineral (Ministry of Education), Northeastern University, Shenyang 110819, P.R. China and also with the School of Metallurgy, Northeastern University, Shenyang 110819, P.R. China. Contact e-mail: dengzy@smm.neu.edu.cn; myzhu@mail.neu.edu.cn XIAOFENG LIU is with the Steel Plant, Chongqing Iron and Steel Co., Ltd., Chongqing 401258, P.R. China.

Manuscript submitted April 18, 2024; accepted June 9, 2024.
Article published online June 27, 2024.

were also studied by the authors.[18] It was found that the TiO_2 in the slags enhanced the dissolution of MgO refractories into the slags, and a higher MgO content in the slags could weaken the dissolution. Furthermore, there are only a few studies considering the effect of TiO_x-containing slag on the cleanliness of steel. For instance, Chen *et al.*[13] indicated that the use of TiO_x-containing slag could reduce the total oxygen content in stainless steel. Zhao *et al.*[19] carried out laboratory studies to investigate the effect of TiO_2 in the slag on the inclusions in Ti-bearing steel, and Ca-Mg-Al-Ti-O complex inclusions, titanium nitrides and carbides were found in the steel after the steel-slag reaction. Due to the large number of steel grades, further studies (especially industrial studies) are still needed to reveal the effect of TiO_x-containing slag on the evolution of inclusions and steel cleanliness.

In addition, alloys are also an important source of inclusions in steel.[20,21] As reported, Ti-Fe alloys generally contain high oxygen and nitrogen content. The high Al content in Ti-Fe alloy may also lead to the generation of titanium aluminate inclusions when alloying. So, improving the cleanliness and reducing the addition of Ti-Fe alloys are conducive to the cleanliness of Ti-bearing steel grades. Because the use of TiO_2-containing slag can improve the yield of Ti alloys, it also presents its significance for steel cleanliness.

In this study, industrial experiments were conducted to investigate the cleanliness of Ti-bearing steel using TiO_2-containing and conventional ladle slags. The evolution of inclusions, the yield of Ti alloy, and the cleanliness of the steel were compared. Based on the experimental results and thermodynamic calculations, some suggestions were made for the refining of Ti-bearing steels.

II. EXPERIMENTS

A. *Process Description and Sampling*

The industrial experiments were carried out in a Chinese steel plant, and the experimental steel grade was Q355, which was produced by the process of "230t basic oxygen furnace (BOF) → 230t ladle furnace (LF) → 230t Ruhrstahl-Hereaeus furnace (RH) → slab continuous casting (CC)". There are two processes, namely Process S1 and Process S2. During the tapping process of BOF, most of the deoxidizers, alloys, and slag formers were charged into the ladle. Especially, in Process S1, around 200 kg TiO_2 was additionally added. At the LF stage, some slag deoxidizers, *e.g.*, Al, were put on the top of the slags for slagging, and some alloys were also added for composition adjustment. It is necessary to mention that in Process S1, the Ti-Fe alloy (70 pct Ti, 3.5 pct O and 0.94 pct N) was added in the RH vacuum chamber when RH started; while it was added at the end of LF refining in Process S2. The time of LF refining was about 60 min, and RH treatment lasted around 20 min. In each process, five pail-type steel samples were taken after tapping (marked as TP), before LF (marked as L1), at the middle stage of LF (marked as L2), at the end of LF (marked as L3) and at the end of RH (marked as R1). Table I gives the detailed compositions of these steel samples. Also, some lollipops were sampled during LF treatment and RH treatment to analyze the variation of Ti content in the steel. In addition, the slags were also sampled at the middle stage of LF (L2), at the end of LF (L3) and at the end of RH (R1), and the compositions of the refining slags of the two processes are listed in Table II.

B. *Analysis*

The steel samples were cut, and their compositions were measured by an inductively coupled plasma-optical emission spectrometer (ICP-OES). The Ca and Mg contents in the steel samples were analyzed by inductively coupled plasma-mass spectrometry (ICP-MS). The total oxygen contents and nitrogen contents were measured by LECO O/N/H analyzer. In addition, the steel samples were prepared for inclusion observation using scanning electron microscopy (SEM, Zeiss EVO 18) with energy-dispersive X-ray spectrometry (EDS). The compositions of the slags were also detected by X-ray fluorescence analysis (XRF).

III. RESULTS

A. *Composition and Nature of Slags*

The composition of each slag sample is given in Table II. As shown in this table, after TiO_2 addition to the refining slag, the TiO_2 content in the slag (Process S1) is 4.28 pct at the middle stage of LF refining. With refining time, the content of TiO_2 decreases slightly. In contrast, the contents of TiO_2 in the slags of Process S2 are lower the 1 pct, and they increase with time. Additionally, it is noted that there is only a very small difference in the slag basicity ($R = w(CaO)/w(SiO_2)$), which ranges from 3.4 to 4.1. The contents of Al_2O_3 in the slags of Process S2 are also slightly higher than the that of Process S1.

Figure 1 shows the photos of the refining slags during LF refining. As shown in this figure, the full liquid nature can be clearly seen in Process S1, while some crusts are formed on the surface of the slag in Process S2. It indicates that the addition of TiO_2 improves the fluidity of the slag.

B. *Composition of Steel Samples*

The compositions of the steel samples are shown in Table I. Figure 2 also plots the Ti contents in the lollipop samples. As shown in Table I and Figure 2, in both processes, the initial Ti content after tapping is only around 20 ppm. In the case of Process S1, the Ti content in the steel gradually increases during LF refining, due to the addition of TiO_2 in this slag. At the middle stage of LF (L2), the Ti content reaches 67 ppm, and it increases slightly to around 72 ppm before Ti-Fe is added in RH. In Process S2, the Ti content almost keeps the same before Ti addition. After Ti alloying in both processes, the Ti contents are about 0.017 pct.

Table I. Compositions of the Steel Samples at Different Stages (Mass Percent, *ppm)

Process	Stage	C	Si	Mn	Cr	Al	Ti	Ca*	Mg*
S1	TP	0.12	0.18	1.30	0.031	0.046	0.0020	0.1	1.2
S1	L1	0.13	0.16	1.31	0.032	0.034	0.0021	0.5	2.0
S1	L2	0.14	0.12	1.36	0.030	0.020	0.0067	0.6	2.8
S1	L3	0.15	0.12	1.39	0.040	0.054	0.0070	0.5	1.2
S1	R1	0.15	0.11	1.39	0.030	0.044	0.0168	2.1	1.3
S2	TP	0.11	0.14	1.05	0.035	0.045	0.0019	0.7	2.1
S2	L1	0.13	0.14	1.30	0.038	0.043	0.0019	0.6	2.5
S2	L2	0.14	0.14	1.39	0.040	0.043	0.0017	0.9	3.7
S2	L3	0.15	0.12	1.38	0.040	0.035	0.0165	0.5	4.7
S2	R1	0.14	0.11	1.36	0.040	0.031	0.0170	1.9	1.5

Table II. Compositions of Experimental Refining Slags (Mass Percent)

Process	Stage	MgO	Al_2O_3	CaO	SiO_2	TiO_2	Basicity R
S1	L2	4.58	23.61	51.72	12.75	4.28	4.1
S1	L3	4.86	24.27	51.52	12.51	4.21	4.1
S1	R1	5.31	24.99	50.10	12.53	4.09	4.0
S2	L2	5.09	28.45	49.56	13.73	0.54	3.6
S2	L3	4.96	29.18	48.66	13.52	0.85	3.6
S2	R1	4.94	28.52	47.28	14.05	0.91	3.4

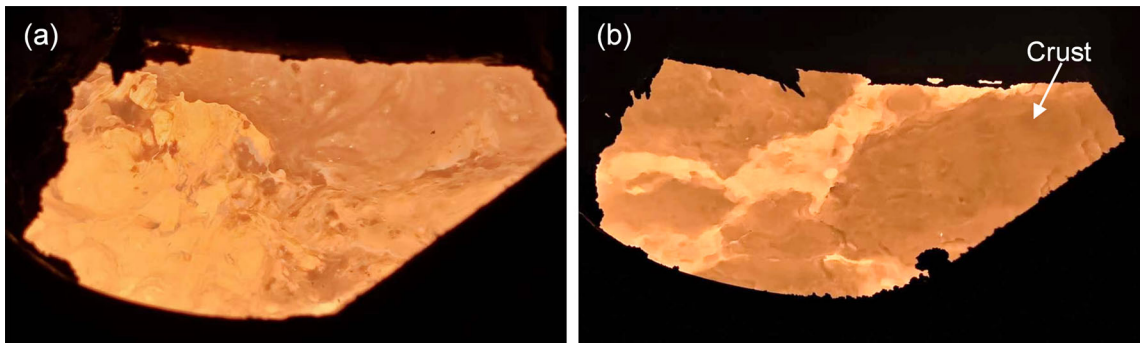

Fig. 1—Photographs of the slags during LF refining. (*a*) TiO_2-containing slag (S1); (*b*) conventional slag (S2).

Figure 3 presents the total oxygen and nitrogen contents of the steel samples. It can be seen from this figure that the total oxygen contents in Process S1 are generally lower than that in Process S2. After RH treatment, the total oxygen contents are only 4 ppm and 5 ppm in Processes S1 and S2, respectively. After casting, the total oxygen contents of the slabs increase to 8 ppm and 11 ppm, respectively. In the case of nitrogen contents, an increasing trend can be found, and Process S1 also obtains a lower content compared with Process S2.

C. *Inclusions in Steel*

1. *Types of inclusions*

Table III lists the types of inclusions at each stage of refining process, and Figures 4 through 8 give the elemental mappings of these types of inclusions. As shown in Table III, Type-I inclusions are Al_2O_3 inclusions, which are mainly found after BOF tapping and at the early stage of LF. In general, they are small in size and irregular in shape, and some of them are in the form of clusters.

As shown in Figure 4, Type-II inclusions are irregular MgO-Al_2O_3 inclusions. They are mainly presented at the middle stage and the end of LF refining, and in the whole process of RH refining. Their sizes are small (5 μm to 10 μm).

The Al_2O_3-TiO_x inclusions are the inclusions of Type-III. As shown in Figure 5, these inclusions are small as well, and they are in both globular and irregular shapes. In Process S1, this type of inclusion is detected since the middle stage of LF refining. While in Process S2, they appear after the addition of Ti-Fe alloy (L3).

The inclusions of Type-IV (*viz.* MgO-Al_2O_3-TiO_x) are observed at the same stage as Type-III inclusions, and the number is very small. This type of inclusion is also mainly composed of MgO-Al_2O_3 spinel, but a small amount of TiO_x is formed at the edge of the inclusions,

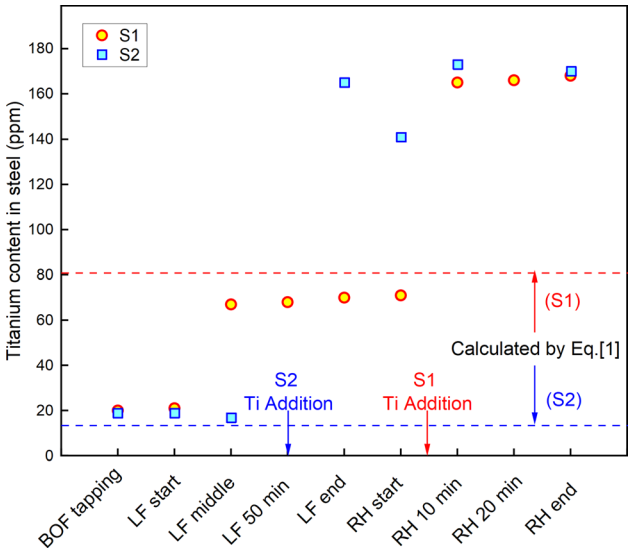

Fig. 2—Ti content in steel during refining process.

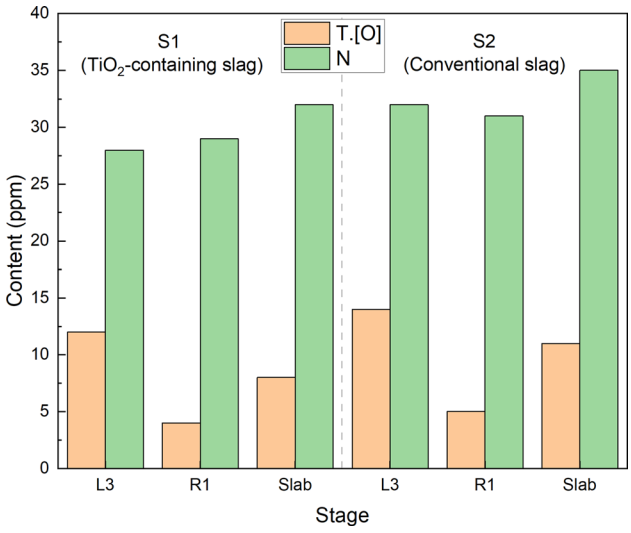

Fig. 3—Total oxygen content and nitrogen content in steel.

see Figure 6. In addition, some MnS-TiS_x can also be found at the edge sometimes, due to the precipitation of sulfide.

Both Type-V and Type-VI inclusions are calcium aluminates. The difference between these two types of inclusions is that only CaO-Al_2O_3(-MgO) phase can be detected in Type-V inclusions as displayed in Figure 7, while some MgO-Al_2O_3 spinel cores exist in Type-VI inclusions, besides the outer phase of CaO-Al_2O_3(-MgO) as shown in Figure 8. These inclusions are generally globular, and their sizes are relatively larger. They can be observed after LF refining process, and further become the main types of inclusion after RH treatment. It is worth noting that a trace of TiO_x can also be detected in these types of inclusions [see Figure 8(b)], but they are still calcium aluminates. This will be discussed in the discussion part.

2. *Composition of inclusions*

The compositions of inclusions at different stages in Processes S1 and S2 are shown in Figures 9 and 10, respectively. In these figures, both CaO-MgO-Al_2O_3 system and MgO-TiO_x-Al_2O_3 system are considered, and the blue lines in the figures are the liquidus at 1600 °C. As reported,[22,23] TiO_x can be represented by Ti_3O_5 at an extremely low oxygen potential. Therefore, the composition of each inclusion is plotted in both CaO-MgO-Al_2O_3 system and MgO-Ti_3O_5-Al_2O_3 system. Also, the overall and the average compositions of inclusions are given in Figures 9(h), (i) and 10(h), (i).

By comparing Figures 9 and 10, it can be seen that the variations of the inclusion compositions are almost the same in Processes S1 and S2. In the CaO-MgO-Al_2O_3 system, after tapping and at the early stage of LF refining, the inclusions in the steel are Al_2O_3 (Type-I) as shown in Figures 9(a) and 10(a); With time, due to the rise of MgO content (below 20 pct) in inclusions, most of the inclusions transform into MgO-Al_2O_3 (Type-II) at the middle and the end of LF refining, see Figures 9(b), (c) and 10(b), (c). Besides, a few CaO-Al_2O_3 (Type-V) and CaO-Al_2O_3-MgO (Type-VI) inclusions are also found in the steel samples. During RH treatment, the MgO content in MgO-Al_2O_3 inclusions further climbs, even up to 30 pct in a few of inclusions. At the same time, the CaO content in some inclusions also increases as shown in Figures 9(d) and (h), 10(d) and (h). In addition, these inclusions move to the region of liquid phase, indicating that they are liquid at steelmaking temperatures.

On the other hand, it can be seen from Figures 9(e) through (g) and 10(e) through (g) that there is a small difference in the TiO_x changing trends in these inclusions. In Process S1, a small amount of TiO_x is generated in inclusions at the middle stage of the LF refining process, as shown in Figures 9(e) and (h). In contrast, only MgO-Al_2O_3 and Al_2O_3 are detected at the same stage in Process S2, as displayed in Figures 10(e) and (h). With refining time, the TiO_x content of inclusions in Process S1 drops again as shown in Figures 9(f) through (h). In Process S2, a small number of TiO_x-containing inclusions are also present due to the addition of Ti-Fe alloys at the end of LF refining, see Figures 10(f) and (h). In both processes, at the end of RH treatment, the TiO_x content of inclusions is very low, as shown in Figures 9(g) through (i) and 10(g) through (i).

3. *Number density of inclusions*

The number density of inclusions in slabs is measured by SEM-EDS using automatic analysis, and the results are given in Table IV. As shown in this table, the number density of inclusions is 25.0 mm^{-2} in Process S1, while it is 31.7 mm^{-2} in Process S2. The number density of inclusions is in line with the trend of total oxygen contents shown in Figure 3.

D. *Yield of Ti Alloy*

Because 72 ppm Ti is already contained in the steel before Ti-Fe addition in Process S1, only 32.0 kg of Fe-Ti alloy is added in the RH vacuum chamber. In the case of Process S2, 57.0 kg of Fe-Ti alloy is added at the

Table III. Composition of Inclusions at Different Stages in Processes S1 and S2

Types	Specification of Inclusions	Stage					
		TP S1/S2	L1 S1/S2	L2 S1	L2 S2	L3 S1/S2	R1 S1/S2
I	Al_2O_3	×××	×××	××	××	××	×
II	$MgO\text{-}Al_2O_3$	—	—	××	××	××	××
III	$Al_2O_3\text{-}TiO_x$	—	—	×	—	×	×
IV	$MgO\text{-}Al_2O_3\text{-}TiO_x$	—	—	×	—	×	×
V	$CaO\text{-}Al_2O_3$(-MgO)	—	—	—	—	×	××
VI	$CaO\text{-}Al_2O_3 + MgO\text{-}Al_2O_3$	—	—	—	—	×	×

"×××"—a large number, "××"—a moderate number, "×"—a small number.

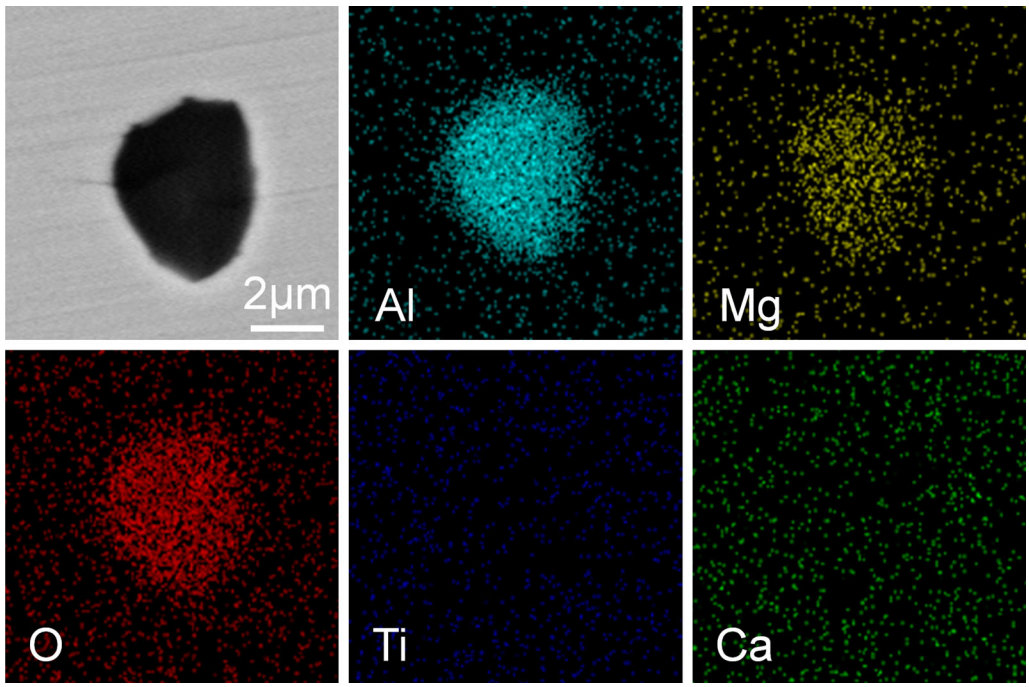

Fig. 4—Elemental mappings of a Type-II inclusion.

end of LF refining. Obviously, the yield of alloy in Process S1 is higher. To be detailed, the yield of the Ti alloys is calculated, and the results are shown in Table IV as well. As shown, the yield in Process S1 is 96.3 pct, which is about 10 pct higher than that in Process S2 (86.5 pct). This is consistent with the trend reported in Reference 13.

IV. DISCUSSION

A. *Estimation of Ti Content Considering Steel-Slag Equilibrium*

It can be seen from Table I and Figure 2 that the Ti content in steel is about 72 ppm before Ti-Fe alloy is added. The rise of Ti content is mainly due to the equilibrium between the TiO_2-containing slag and steel. In this case, the [Ti]-[O] equilibrium can be considered to estimate the Ti content. In literature,[24] Ti_2O_3 and Ti_3O_5 were considered based on different Ti contents in steel. In this study, although TiO_2 was added in the slags in Process S1, considering the atmosphere of LF refining and the alloys in steel, Ti_3O_5 is chosen to represent the TiO_x in the slag, and Eq. [1] is employed to calculate the equilibrated Ti content. The thermodynamic data are given in Table V.

$$(Ti_3O_5) = 3[Ti] + 5[O] \quad [1]$$

In general, the dissolved oxygen activity is around 3 ppm after Al addition in the case of the experimental steel grades. At the same time, the activity of the dissolved oxygen was also reported as around 3 ppm when the Al content is about 0.04 pct.[5,35] Based on the dilute solution model, the activity of Ti in steel can be

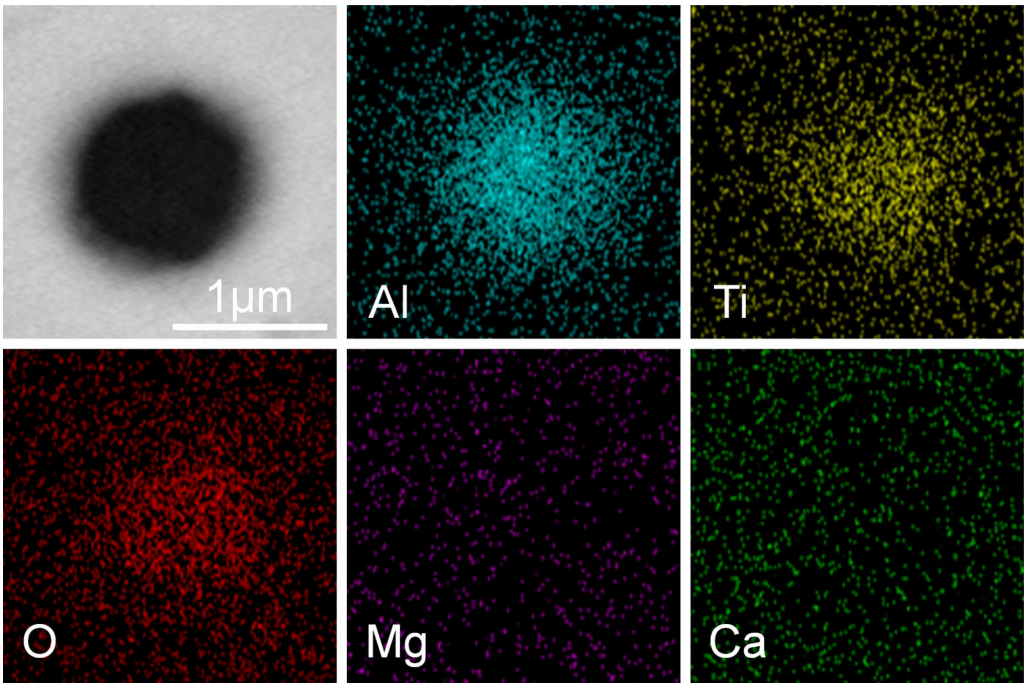

Fig. 5—Elemental mappings of a Type-III inclusion.

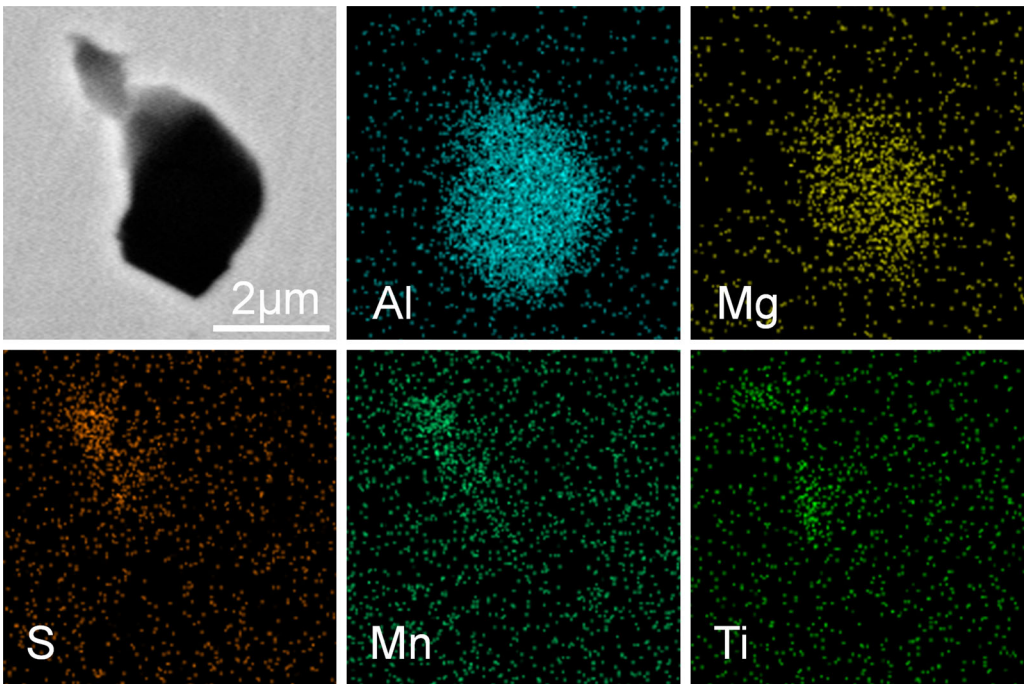

Fig. 6—Elemental mappings of a Type-IV inclusion.

calculated based on the Ti content and the activity coefficient using the data given in Table VI. The activities of the Ti_3O_5 in the slags (L2) are estimated by thermodynamic calculation software FactSage 7.3 using the FToxid database, *viz.* 1.73×10^{-8} and 8.15×10^{-11} for Processes S1 and S2, respectively. Therefore, the calculated Ti contents when in equilibrium are 81.0 ppm and 13.6 ppm in the two processes, respectively. The calculated values are marked in Figure 2 for comparison, and it is found that the measured

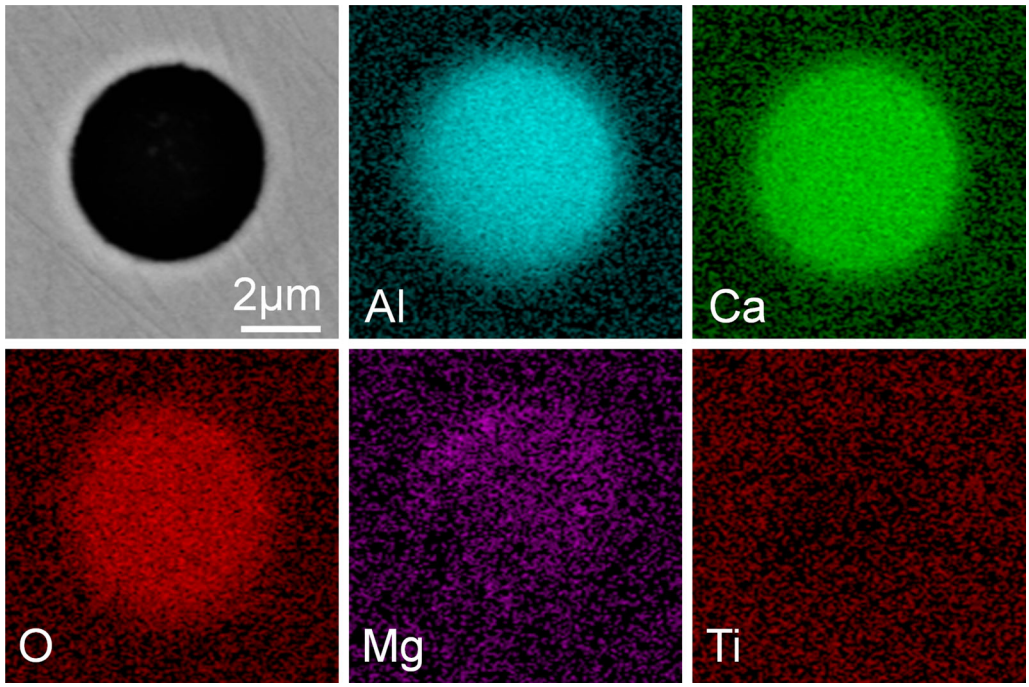

Fig. 7—Elemental mappings of a Type-V inclusion.

values are very close to the calculated ones before Ti addition in both processes. From thermodynamic aspect, the addition of TiO_2 in the slag can lead to much higher Ti content in steel.

B. *Evolution of Inclusions*

Several studies indicated that the inclusions in Ti-bearing Al-killed steel (Ti 0.07 pct) transformed from Al_2O_3 inclusions into MgO-Al_2O_3 spinel and further into MgO-Al_2O_3-TiO_x system inclusions after Ti addition. When the Ca content in steel increased to a certain extent, the inclusions changed into CaO-Al_2O_3-TiO_x and even CaO-TiO_x system inclusions.[5] In this study, as shown in Figures 9(e) through (h) and 10(f) through (h), some TiO_x can also be detected in the inclusions. Even though, the TiO_x content of inclusions drops with time, and the inclusions become MgO-Al_2O_3 (Type-II) and CaO-Al_2O_3 systems (Type-V and Type-VI) at the end of RH refining. This difference in the evolution of inclusions probably depends on the different compositions of the steel grades. In order to check this reasoning, thermodynamic calculations and considered to calculate the phase stability diagram of different inclusions.

As reported,[35,37,38] Eqs. [2], [4] and [6] can be employed to draw the phase stability diagram of Al_2O_3/MgO·Al_2O_3/MgO·Ti_2O_3. The Gibbs free energies are calculated based on the data listed in Table V. The activities of dissolved Al, Mg and Ti in steel are also estimated by the dilute solution model, and the activities of Al_2O_3, MgO, MgO·Al_2O_3 and MgO·Ti_2O_3 are considered as unity. In addition, the dissolved O and Mg in steel are set as 3 ppm and 2 ppm, respectively.

$$3MgO \cdot Al_2O_3 + 2[Al] = 4Al_2O_3 + 3[Mg] \quad [2]$$

$$\Delta G_2^0 = -540936 + 487.4T \ \text{(J/mol)} \quad [3]$$

$$4MgO + 2[Al] = MgO \cdot Al_2O_3 + 3[Mg] \quad [4]$$

$$\Delta G_4^0 = -616248 + 462.2T \ \text{(J/mol)} \quad [5]$$

$$MgO \cdot Al_2O_3 + 2[Ti] = MgO \cdot Ti_2O_3 + 2[Al] \quad [6]$$

$$\Delta G_6^0 = 3262551 - 134T \ \text{(J/mol)} \quad [7]$$

Figure 11 gives the calculated stability phase diagram of Al_2O_3/MgO·Al_2O_3/MgO·Ti_2O_3. Meanwhile, the measured Al and Ti contents are plotted in this figure. In this study, the Ti content is about 0.017 pct, therefore it can be seen from this figure that MgO·Al_2O_3 is the stable phase before and after Ti addition in the experimental steel grade. In fact, this is different from the results in the previous studies.[5] It implies that the Ti content in steel holds the key to this difference. It is also necessary to mention that a few Al_2O_3-TiO_x (Type-III) and MgO-Al_2O_3-TiO_x (Type-IV) inclusions are found, but the content of TiO_x in the inclusions is still low as given in Figures 9(h) and 10(h). Because those inclusions also transform into MgO-Al_2O_3 and CaO-Al_2O_3

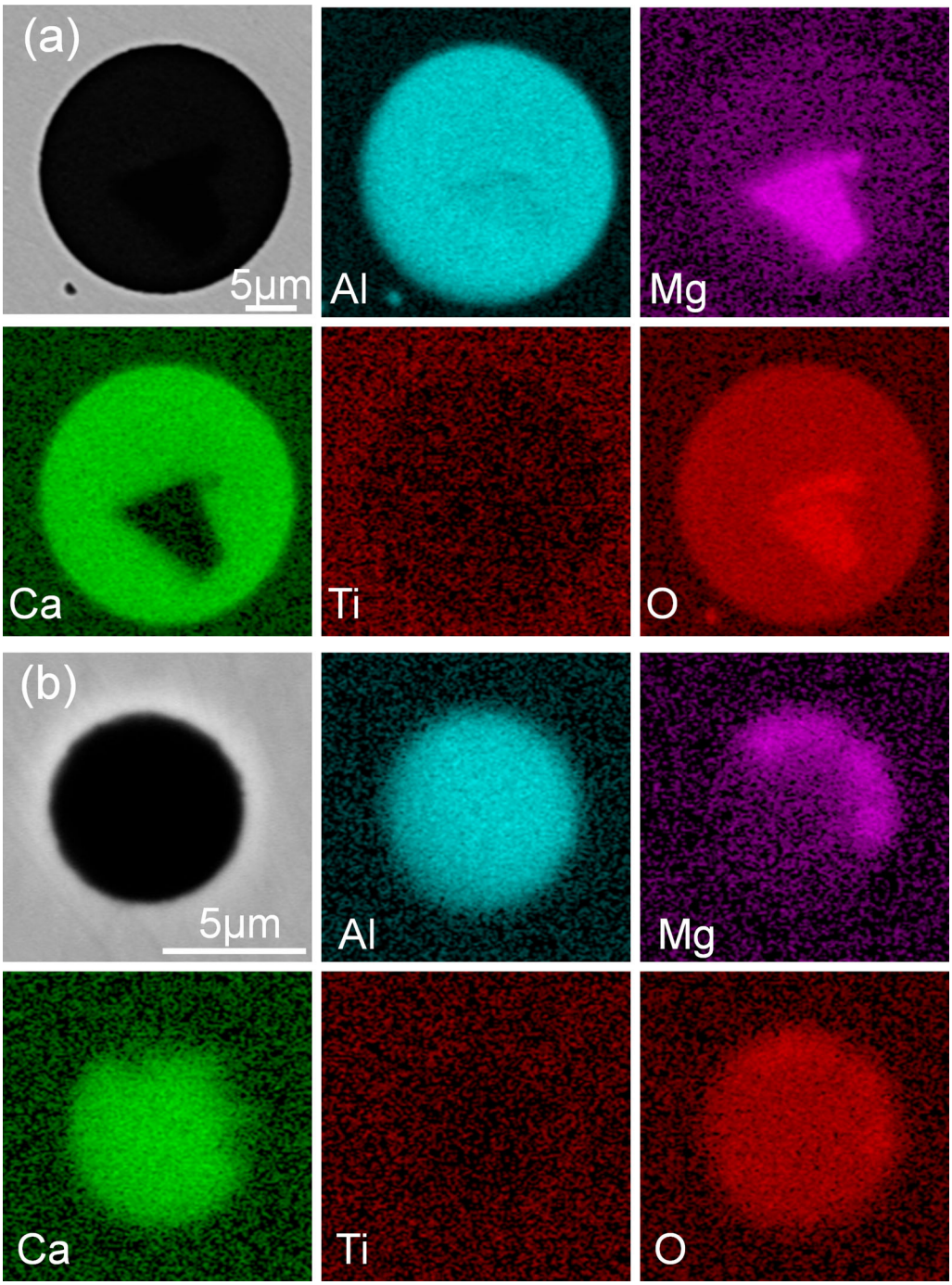

Fig. 8—Elemental mappings of a Type-VI inclusion.

systems as mentioned above, it further improves that $MgO\text{-}Al_2O_3$ is the stable phase when dissolved Ca in steel is not taken into account.

As shown in Figures 7 through 10, some $CaO\text{-}Al_2O_3$ system inclusions (Type-V and Type-VI) are observed after LF treatment and RH treatment. It can be seen from Table I that the Ca content is extremely low during LF treatment, and then it increases to around 2 ppm after RH treatment. There are many publications[5,35,37] pointing out that $MgO\text{-}Al_2O_3$ inclusions would transform into $CaO\text{-}Al_2O_3$ inclusions when a trace of Ca is presented in steel. Therefore, the formation of $CaO\text{-}Al_2O_3$ system inclusions seems reasonable in this study. Considering the effect of Ti in the steel, the

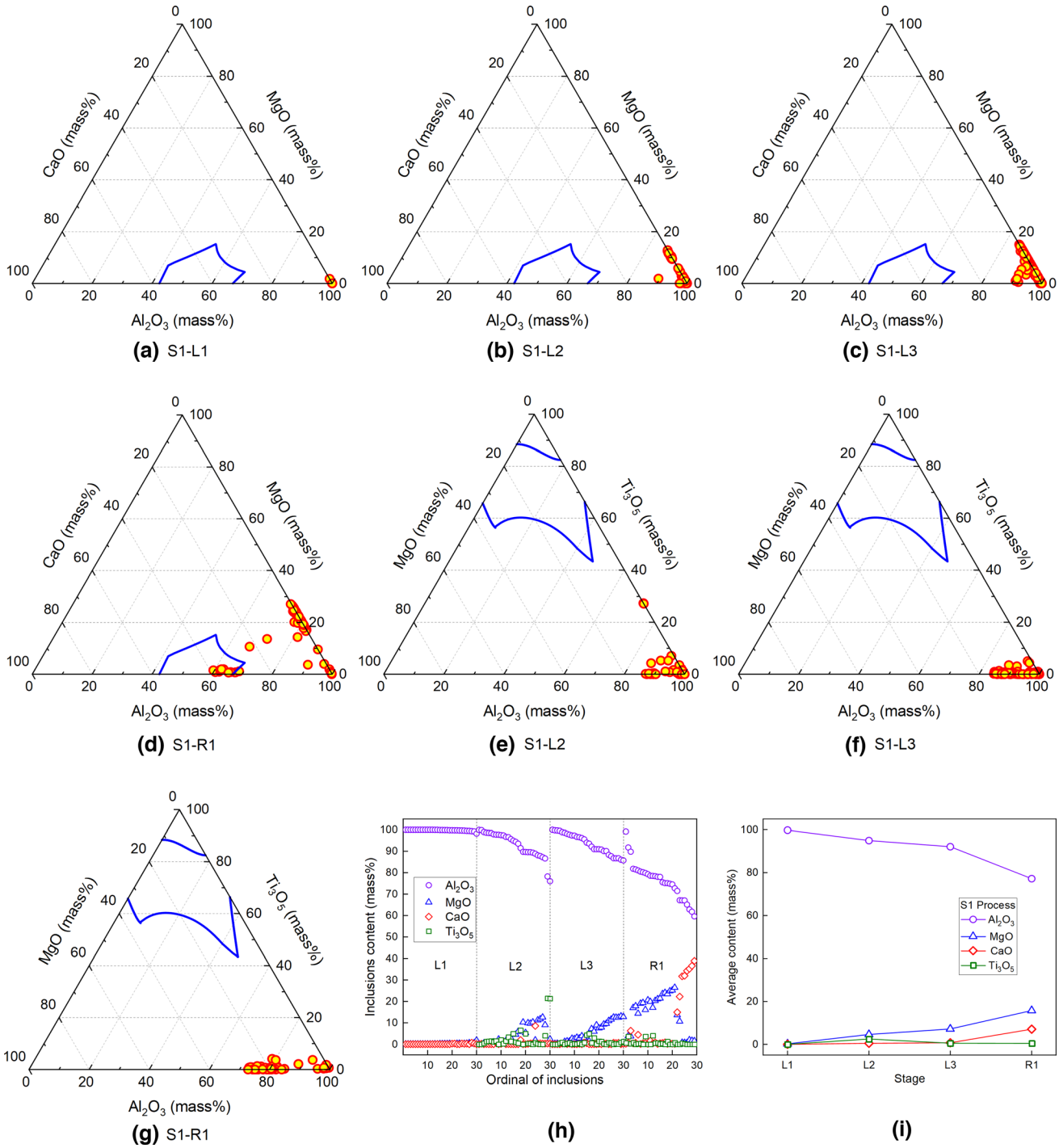

Fig. 9—Composition of inclusions at different stages in Process S1. (*a*) to (*d*): plotted in CaO-MgO-Al_2O_3 system (L1 to R1); (*e*) to (*g*): plotted in MgO-TiO_x-Al_2O_3 system (L2 to R1); (*h*) composition of each inclusion; (*i*) average composition.

stability between $CaO{\cdot}Al_2O_3$ and $CaO{\cdot}TiO_2$ inclusions also needs to be checked using Eq. [8]. It is calculated that the Gibbs free energy (ΔG) of Eq. [8] is 125.8 kJ/mol, and this value proves that CaO-Al_2O_3 inclusions are more stable than CaO-TiO_2 inclusions.

In this case, the phase stability diagram of Al_2O_3/$CaO{\cdot}Al_2O_3$/$MgO{\cdot}Al_2O_3$ shown in Figure 12 can also be calculated using Eqs. [2], [10] and [12] by referring to a previous study of the authors.[5] The measured Ca and Mg contents are also plotted in Figure 12. According to

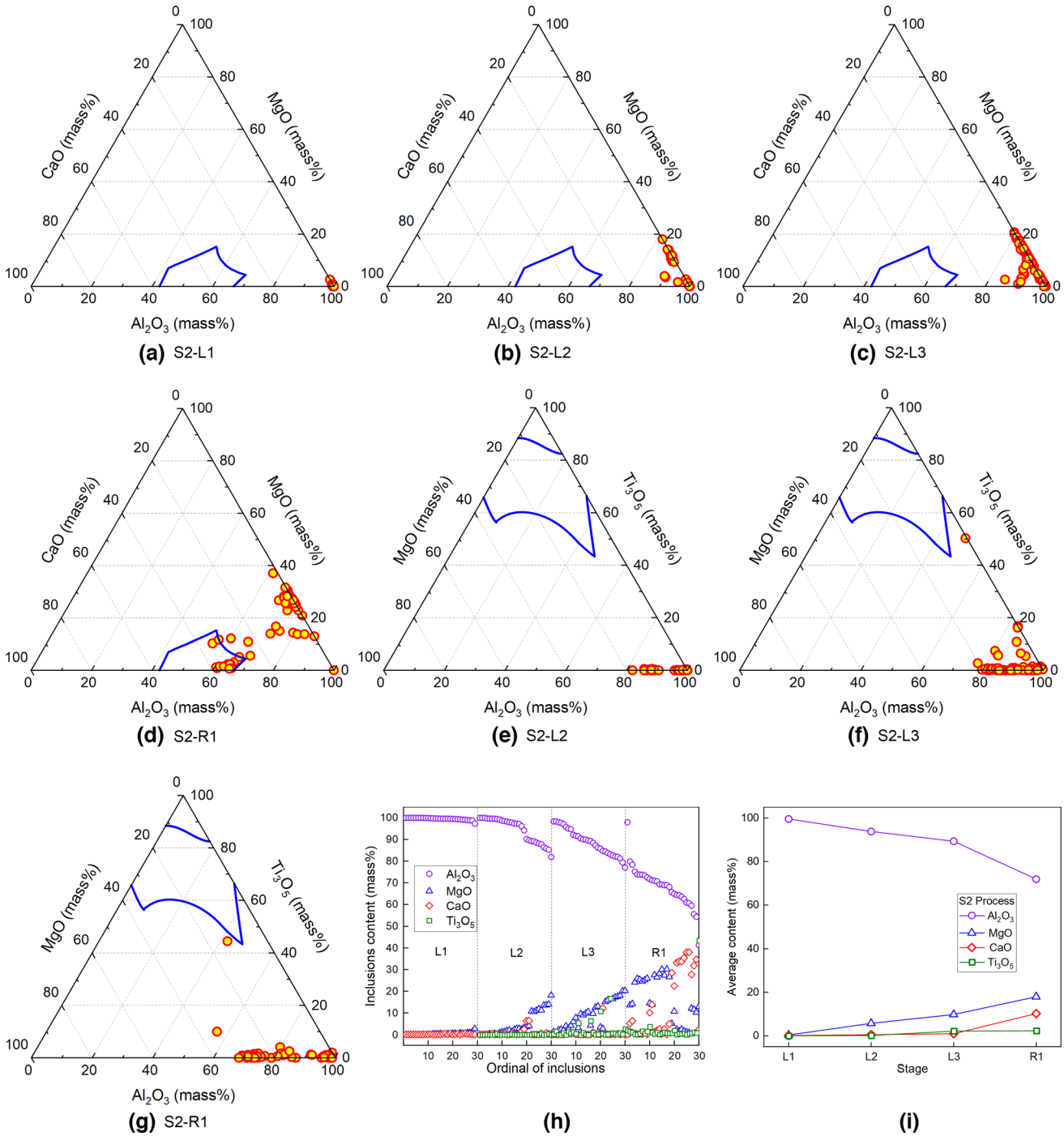

Fig. 10—Composition of inclusions at different stages in Process S2. (*a*) to (*d*): plotted in CaO-MgO-Al_2O_3 system (L1 to R1); (*e*) to (*g*): plotted in MgO-TiO_x-Al_2O_3 system (L2 to R1); (*h*) composition of each inclusion; (*i*) average composition.

Figure 12, it is confirmed that the stable inclusions are CaO-Al_2O_3 system when the Ti content is 0.017 pct. This means that MgO·Al_2O_3 inclusions should transform into CaO-Al_2O_3 system inclusions when a trace of Ca (even 2 ppm) is generated in the steel. On the other hand, due to the low Ti content in steel, CaO·TiO_2 inclusions can hardly be formed, even if the Ca content in steel is sufficiently high.

$$3CaO \cdot Al_2O_3 + 4[Ti] + [Ca] = 4CaO \cdot TiO_2 + 6[Al] \quad [8]$$

$$\Delta G_8^0 = -504610 + 271T \ (J/mol) \quad [9]$$

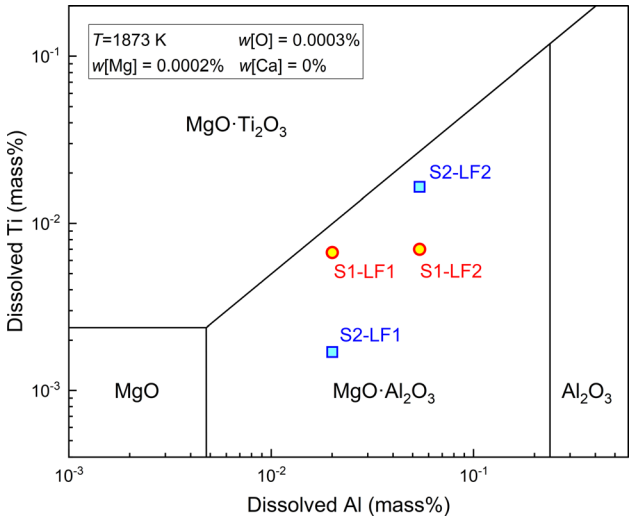

Fig. 11—Phase stability diagram of Al_2O_3/MgO·Al_2O_3/MgO·Ti_2O_3.

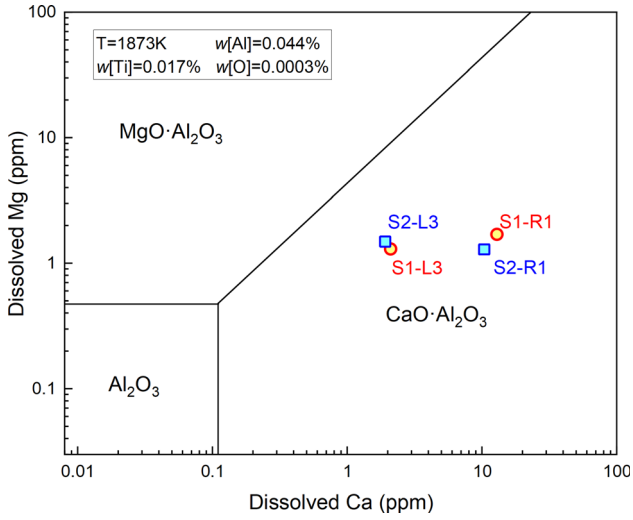

Fig. 12—Stability phase diagram of Al_2O_3/CaO·Al_2O_3/MgO·Al_2O_3.

Table IV. Number Density of Inclusions and Ti Yield in Processes S1 and S2

Process	Number Density of Inclusions (mm^{-2})	Ti-Fe Alloy Addition (kg)	Ti Yield (pct)
S1	25.0	32.0	96.3
S2	31.7	57.0	86.5

Table V. Gibbs Free Energies of the Reactions

Reactions	ΔG^0(J/mol)	Refs.
TiO_2 = [Ti] + 2[O]	$675600 - 234T$	25
Ti_2O_3 = 2[Ti] + 3[O]	$822000 - 247.7T$	26
Ti_3O_5 = 3[Ti] + 5[O]	$1307000 - 381.8T$	26
Al_2O_3 = 2[Al] + 3[O]	$867300 - 222.5T$	27
CaO = [Ca] + [O]	$138240 + 63T$	28
MgO = [Mg] + [O]	$89960 + 82T$	29
MgO·Al_2O_3 = MgO + Al_2O_3	$18828 + 6.3T$	30
CaO·TiO_2 = CaO + TiO_2	$79900 - 3.35T$	31
CaO·Al_2O_3 = CaO + Al_2O_3	$17910 + 17.38T$	32
Al_2O_3·TiO_2 = [Ti] + 2[Al] + 5[O]	$1435000 - 400.5T$	33
MgO·Ti_2O_3 = [Mg] + 2[Ti] + 4[O]	713537 (1873K)	34

Table VI. Interaction Coefficient e_i^j of Dissolved Element in Steel[5,36]

	j								
i	C*i*	Si	Mn	Cr	Al	O	Ti	Mg	Ca
Al	0.091	0.056	− 0.004	0.012	0.045	− 1.98	0.016	− 0.13	− 0.047
Mg	0.15	− 0.096	—	0.05	− 0.12	− 460	− 0.64	—	—
Ca	− 0.34	− 0.096	− 0.007	0.014	− 0.072	− 780	− 0.13	− 0.13	− 0.002
Ti	− 0.19	− 0.025	− 0.043	0.0158	0.037	− 3.4	0.042	− 1.27	− 0.157
O	− 0.421	− 0.066	− 0.021	− 0.055	− 1.17	− 0.17	− 0.44	− 300	− 515

$$Al_2O_3 + [Ca] + [O] = CaO \cdot Al_2O_3 \quad [10]$$

$$\Delta G^0_{10} = -156150 - 80.38T \ \text{(J/mol)} \quad [11]$$

$$MgO \cdot Al_2O_3 + [Ca] = CaO \cdot Al_2O_3 + [Mg] \quad [12]$$

$$\Delta G^0_{12} = -47362 + 7.92T \ \text{(J/mol)} \quad [13]$$

It is noted that in Figures 9(h), (i) and 10(h), (i), both $MgO\text{-}Al_2O_3$ (Type-II) and $CaO\text{-}Al_2O_3$ systems (Type-V and Type-VI) are observed after LF treatment and RH treatment. It seems that the experimental results are not consistence with the thermodynamic calculations. In fact, this can be explained from the aspect of kinetics. Before the sufficient generation of Ca in liquid steel, $MgO\text{-}Al_2O_3$ (Type-II) inclusions are the stable phase, so the MgO content in the inclusions should be increased. When the stable phase changes into $CaO\text{-}Al_2O_3$ system, the evolution of $MgO\text{-}Al_2O_3$ into $CaO\text{-}Al_2O_3$ needs to take place, leading to the rise of CaO content in inclusions. As reported in literature,[5,35] the reaction of Eq. [12] is the mechanism. Because the Ca in steel is still low as given in Table I, this transformation takes some time. As a result, $MgO\text{-}Al_2O_3$ (Type-II) and $CaO\text{-}Al_2O_3$ (Type-V and Type-VI) inclusions coexist in steel, and both the average contents of CaO and MgO are higher than that at an earlier stage. This doesn't change the evolution route of inclusions.

C. *Influence of TiO_2 Addition on Steel Cleanliness*

As shown in Figure 3, the total oxygen and nitrogen contents in steel are reduced by using TiO_2-containing slag. By checking the inclusions detected by SEM, the number density of inclusions in Process S1 is also lower than that in Process S2, see Table IV. These results indicate that the steel cleanliness is improved by the addition of TiO_2 in the slag.

It is also noted that after the addition of TiO_2 in the slag in Process S1, the addition of Ti-Fe alloy is also reduced as shown in Table IV. As mentioned earlier, the Ti-Fe alloy contains a high total oxygen content (3.5 pct) and a high nitrogen content (0.94 pct), so the smaller addition of Ti-Fe alloy in steel reduces the pollution of the impurities in the alloy. In this case, better steel cleanliness should be reasonable.

On the other hand, as shown in Figure 1, the slag properties are improved after the addition of TiO_2 in the slag in Process S1. In fact, the laboratory studies of the authors[16–18] also confirmed this effect of TiO_2. It is found that a suitable addition of TiO_2 (*e.g.*, 5 pct) in refining slags could lower the melting point and the viscosity of the slags. As reported in literature,[39,40] lower melting point and viscosity are beneficial for the removal of inclusions. In this case, the slag in Process S1 plays an important role in the lower total oxygen content as well.

It is also noted that in this study, the slag basicity is in the range of 3.4~4.1. Even though, the total oxygen contents after RH treatment are around 5 ppm, which are extremely low. Some researchers[37,41] proposed that ultra-high basicity is good for steel cleanliness. They believed that the slag can accelerate the evolution of inclusions, and the generated liquid calcium aluminate inclusions can be easily removed, thus improving steel cleanliness. In contrast, the present authors[4,35] and some researchers[42] found that the removal of solid inclusions (*e.g.*, Al_2O_3 and $MgO\text{-}Al_2O_3$) is much easier than that of liquid inclusions, due to the huge difference in the separation behaviors at the steel-slag interface. Considering the evolution route of inclusions, $MgO\text{-}Al_2O_3$ inclusions are suggested to be removed before they transform into liquid calcium aluminates. It is reported[4,35,42] that most of solid inclusions can be removed in RH, therefore suitable slag basicity is necessary to control most of the inclusions to be solid $MgO\text{-}Al_2O_3$ in RH. In the earlier publication of the authors,[43] slag basicity of around 4 is suggested for ultra-low oxygen steels. In this study, the low total oxygen contents further prove this possibility. Although there is a difference in the basicity in Process S1 and Process S2, the differences in the CaO and SiO_2 contents in the slags are still small (up to 2 pct). Therefore, the basicity difference in these processes cannot lead to an evident difference in total oxygen contents in the steel. As shown in Table III and Figures 9, 10, $MgO\text{-}Al_2O_3$ inclusions (Type-II) are the dominant type of inclusions after RH treatment. The evolution of inclusions in this study also confirms that suitable slag basicity could control most of the inclusions to be solid state. Furthermore, by comparing Process S1 and Process S2, it can be seen that the addition of TiO_2 in the slag doesn't change the evolution of inclusions evidently. From this aspect, the addition of TiO_2 can hardly weaken the removal efficiency of inclusions in this study. Instead, it can play a positive role due to the effect on the properties of the slag.

It is necessary to mention that the Ti content is around 170 ppm in the experimental steel. In fact, for different Ti-bearing steel grades, the Ti content should be different. As discussed above, the evolution of inclusions may be influenced by the Ti content in steel. Therefore, the effect of the TiO_2-containing slag on the inclusions in steel needs further investigation for different Ti-bearing steel grades.

V. CONCLUSIONS

In this study, the effect of TiO_2 addition on the evolution of nonmetallic inclusions in Ti-bearing Al-killed steel was investigated. Based on the industrial studies and thermodynamic analysis, the main conclusions are obtained as follows:

(1) Suitable addition of TiO_2 can improve the fluidity of the slag, thereby enhancing the refining effect. When using TiO_2-containing slag, the Ti content increases to 72 ppm in steel during LF refining due to [Ti]-[O] equilibrium, and the yield of Ti-Fe alloy also climbs from 86.5 pct to 96.3 pct in RH refining even with a lower addition amount. In this case, the steel cleanliness is improved together with lower total oxygen and nitrogen contents as well as a smaller number density of inclusions in steel.
(2) There is no evident difference in the evolution of inclusions. In both processes, the inclusions generally transform from Al_2O_3 into $MgO\text{-}Al_2O_3$, and even liquid $CaO\text{-}Al_2O_3$ inclusions. Although a small amount of TiO_x is generated in inclusions at the middle of LF due to the effect of TiO_2-containing slag, solid $MgO\text{-}Al_2O_3$ inclusions are still the dominant inclusions in steel after RH refining. Therefore, suitable addition of TiO_2 does not evidently influence the evolution of inclusions, and it can hardly weaken the removal efficiency of inclusions. In fact, it helps the removal of inclusions due to its effect on slag properties.

ACKNOWLEDGMENTS

The National Natural Science Foundation of China (Grant Nos. U20A20272 and 52074073) and the Fundamental Research Funds for the Central Universities (No. 2325035) were acknowledged for the financial support of this study.

CONFLICT OF INTEREST

No potential conflict of interest was reported by the authors.

REFERENCES

1. Z.B. Yang, F.M. Wang, S. Wang, and B. Song: *Steel Res. Int*., 2008, vol. 79, pp. 390–95.
2. J.S. Byun, J.H. Shim, Y.W. Cho, and D.N. Lee: *Acta Mater*., 2003, vol. 51, pp. 1593–1606.
3. J.H. Shim, Y.J. Oh, J.Y. Suh, Y.W. Cho, J.D. Shim, J.S. Byun, and D.N. Lee: *Acta Mater*., 2001, vol. 49, pp. 2115–122.
4. M.Y. Zhu and Z.Y. Deng: *Acta Metall. Sin*., 2022, vol. 58, pp. 28–44.
5. Z.Y. Deng, L. Chen, G.D. Song, and M.Y. Zhu: *Metall. Mater. Trans. B*, 2020, vol. 51, pp. 173–86.
6. C. Wang, N.T. Nuhfer, and S. Sridhar: *Metall. Mater. Trans. B*, 2009, vol. 40, pp. 1022–34.
7. S. Basu, S.K. Choudhary, and N.U. Girase: *ISIJ Int*., 2004, vol. 10, pp. 1653–60.
8. H. Cui, Y. Bao, M. Wang, and W. Wu: *Int. J. Miner. Metall. Mater*., 2010, vol. 17, pp. 154–58.
9. P. Dorrer, S.K. Michelic, C. Bernhard, A. Penz, and R. Rossler: *Steel Res. Int*., 2019, vol. 90, p. 1800635.
10. Y. Li, G.G. Cheng, J.L. Lu, and J. Sun: *ISIJ Int*., 2022, vol. 62, pp. 2266–75.
11. M.A. Van Ende, M.X. Guo, R. Dekkers, M. Burty, J. Van Dyck, P.T. Jones, B. Blanpain, and P. Wollants: *ISIJ Int*., 2009, vol. 49, pp. 1133–40.
12. W. Yang, Y. Zhang, L.F. Zhang, H.J. Duan, and L. Wang: *J. Iron. Steel Res. Int*., 2015, vol. 12, pp. 1069–77.
13. X.R. Chen, G.G. Cheng, Y.Y. Hou, J.Y. Li, and J.X. Pan: *J. Iron. Steel Res. Int*., 2020, vol. 27, pp. 913–21.
14. J.Y. Li and G.G. Cheng: *ISIJ Int*., 2019, vol. 59, pp. 2013–23.
15. Y. Wang, J.H. Cho, T.S. Jeong, A. Karasev, W.Z. Mu, J.H. Park, and P.G. Jonsson: *Metall. Mater. Trans. B*, 2021, vol. 52, pp. 3986–4001.
16. X.M. Zhang, Z.W. Yan, Z.Y. Deng, and M.Y. Zhu: *Metals*, 2023, vol. 13, p. 431.
17. X.M. Zhang, Z.Y. Deng, Z.W. Yan, C.X. Wei, and M.Y. Zhu: *Metall. Mater. Trans. B*, 2024, vol. 55, p. 1656.
18. G.Y. Hao, Z.Y. Deng, C.X. Wei, and M.Y. Zhu: *Metall. Mater. Trans. B*, 2023, vol. 54, pp. 3203–15.
19. M.G. Zhao, H. Liu, X.F. Wang, G.J. Chen, Q.Q. Wang, X.B. Zhang, and S.P. He: *Steel Res. Int*., 2022, vol. 93, p. 2200239.
20. G.Y. Hao, K. Yuan, J. Gao, Z.Y. Deng, and M.Y. Zhu: *Iron Steel*, 2020, vol. 55, pp. 37–49.
21. Y. Wang, A. Karasev, J.H. Park, and P.G. Jönsson: *Metall. Mater. Trans. B*, 2021, vol. 52, pp. 2892–2925.
22. W.Y. Cha, T. Nagasaka, T. Miki, Y. Sasaki, and M. Hino: *ISIJ Int*., 2006, vol. 46, pp. 996–1005.
23. S.H. Seok, T. Miki, and M. Hino: *ISIJ Int*., 2011, vol. 51, pp. 566–72.
24. W.Y. Cha, T. Miki, Y. Sasaki, and M. Hino: *ISIJ Int*., 2008, vol. 48, pp. 729–38.
25. T. Hong and T. Debroy: *Scripta Mater*., 2001, vol. 44, pp. 847–52.
26. Y. Li, T. Zhang, and H. Duan: *Metals*, 2019, vol. 9, p. 104.
27. H. Itoh, M. Hino, and S. Ban-ya: *Tetsu-to-Hagané*, 1997, vol. 83, pp. 773–78.
28. H. Itoh, M. Hino, and S. Ban-ya: *Tetsu-to-Hagané*, 1997, vol. 83, pp. 695–700.
29. H. Itoh, M. Hino, and S. Ban-ya: *Tetsu-to-Hagané*, 1997, vol. 83, pp. 623–28.
30. H.R. Rein and J. Chipman: *Trans. Metall. Soc. AIME*, 1965, vol. 233, p. 415.
31. E.T. Turkdogan: *Physical Chemistry of High Temperature Technology*, Academic Press, New York, 1980, p. 8.
32. K. Nagata, J. Tanabe, and K.S. Goto: *Tetsu-to-Hagané*, 1989, vol. 75, pp. 2023–30.
33. H. Matsuura, C. Wang, G. Wen, and S. Sridhar: *ISIJ Int*., 2007, vol. 47, pp. 1265–74.
34. H. Ono, K. Nakajima, R. Maruo, S. Agawa, and T. Usui: *ISIJ Int*., 2009, vol. 49, pp. 957–64.
35. Z.Y. Deng and M.Y. Zhu: *ISIJ Int*., 2013, vol. 53, pp. 450–58.
36. The Japan Society for the Promotion of Science, the 19th Committee on Steelmaking: *Steelmaking Data Sourcebook*, Gordon and Breach Science Publishers, New York, 1988.
37. M. Jiang, X.H. Wang, B. Chen, and W.J. Wang: *ISIJ Int*., 2010, vol. 50, pp. 95–104.
38. Y. Ren, L.F. Zhang, W. Yang, and H. Duan: *Metall. Mater. Trans. B*, 2014, vol. 45B, pp. 2057–71.
39. A.B. Fox, M.E. Valdez, J. Gisby, R.C. Atwood, P.D. Lee, and S. Sridhar: *ISIJ Int*., 2004, vol. 44, pp. 836–45.
40. Y. Ren, P. Zhu, C. Ren, N. Liu, and L. Zhang: *Metall. Mater. Trans. B*, 2022, vol. 53, pp. 682–92.
41. H. Todoroki and K. Mizuno: *ISIJ Int*., 2004, vol. 44, pp. 1350–57.
42. N. Kikuchi: *ISIJ Int*., 2020, vol. 60, pp. 2731–44.
43. Z.Y. Deng and M.Y. Zhu: *ISIJ Int*., 2014, vol. 54, pp. 1498–1506.

Publisher's Note Springer Nature remains neutral with regard to jurisdictional claims in published maps and institutional affiliations.

Springer Nature or its licensor (e.g. a society or other partner) holds exclusive rights to this article under a publishing agreement with the author(s) or other rightsholder(s); author self-archiving of the accepted manuscript version of this article is solely governed by the terms of such publishing agreement and applicable law.